

SPTCStencil: Using Sparse Tensor Cores for Stencil Computation

Qiqi Gu*
qiqi.gu@sjtu.edu.cn
Shanghai Jiao Tong University
Shanghai, China

Heng Shi†
heng.shi@sjtu.edu.cn
Shanghai Enflame Technology Co.Ltd; Shanghai Jiao Tong
University
Shanghai, China

Chenpeng Wu*
cpwu_sjtu@sjtu.edu.cn
Shanghai Jiao Tong University
Shanghai, China

Jianguo Yao†
jianguo.yao@sjtu.edu.cn
Shanghai Jiao Tong University
Shanghai, China

Abstract

Stencil computation, a pivotal numerical method in science and engineering, iteratively updates grid points using weighted neighbor contributions and exhibits strong parallelism for multi-core processors. Current optimization techniques targeting conducting stencil computation on tensor core accelerators incur substantial overheads due to redundant zero-padding during the transformation to matrix multiplication. To address this, we introduce a sparse computation paradigm that eliminates inefficiencies by exploiting specialized hardware units.

This paper exploits the sparsity in these matrices as a feature and presents SPTCStencil, a high-performance stencil computation system accelerated by Sparse Tensor Core (SpTCs). SPTCStencil is the first to harness SpTCs for acceleration beyond deep learning domains. First, Our approach generalizes an efficient transformation of stencil computation into matrix multiplications and specializes this conversion for SpTC compatibility through a novel sparsification strategy. Furthermore, SPTCStencil incorporates a high-performance GPU kernel with systematic optimizations designed to maximize efficiency on SpTCs. Experimental evaluations demonstrate that SPTCStencil 5.46× and Tensor Core-based approaches by 2.00× on average.

Keywords: Stencil Computation, Sparse Tensor Core, High Performance Computing, Matrix Multiplication

1 Introduction

Stencil Computation, characterized as one of seven most critical numerical methods in science and engineering by scientists from Berkeley[5, 14], is widely used across domains, including fluid dynamics[23, 29], earth modeling[24], weather simulations[4, 6], wave equation[3, 34]. It updates

the points inside a grid (also known as *stencil input*) by applying a predefined pattern of weighted contributions from their neighboring points. Specifically, the updated value at a given location is computed as a linear combination of its adjacent elements, where each neighbor’s contribution is scaled by a corresponding coefficient. This operation is iteratively applied across the computational domain until convergence is achieved, with the values at each time step derived from the results of the preceding time step.

The inherent independence in updating individual points makes stencil computation highly suitable for parallel execution on multi-core CPU and GPU architectures, where each thread can be assigned to update specific partitions. However, its high spatial locality makes designing an efficient algorithm on these multi-core processors a non-trivial task, since it may cause significant memory overhead by redundantly loading neighboring points for each point’s update. To address this challenge, researchers have developed various optimization techniques focused on improving data reuse[15, 33]. The most widely adopted approach is tiling[36, 39, 42], which partitions nested loops into smaller tiles to improve data locality by prefetching and caching data blocks before processing subsequent tiles. Furthermore, vectorization techniques [21, 26] have been explored, employing loop unrolling and data layout transformations to optimize the utilization of Single Instruction Multiple Data (SIMD) units in modern processors.

The recent emergence of specialized arithmetic logic units (ALUs) has opened new avenues for stencil computation acceleration. Notably, *Tensor Cores*, specifically designed to accelerate matrix multiplication operations, are highly promising, delivering up to 4× higher throughput compared to traditional CUDA Cores. This architectural advancement has inspired a new research direction that reformulates stencil computations as matrix multiplication problems to exploit Tensor Cores for acceleration. Recent studies[11, 28, 49] have made significant progress in this domain. The pioneering

*Equal Contribution

†Corresponding author

work TCStencil[28] has paved the way for transforming stencil operations into matrix multiplications that are compatible with Tensor Cores, yielding notable performance improvements. Subsequent innovations, including ConvStencil[11] and LoRAStencil[49], have advanced this paradigm through optimized memory access patterns, thereby accelerating the computation further.

Existing solutions leveraging Tensor Cores for stencil acceleration inevitably introduce excessive zero-padding when converting stencil computation to matrix multiplication. Despite the presence of these padded zero values, such approaches continue to employ dense computation paradigms. This strategy overlooks the inherent structured sparsity introduced by the transformation, consequently leading to substantial redundant computation and memory access overhead. In contrast, we recognize that adopting sparse computation paradigms can significantly mitigate these inefficiencies. Specifically, by carefully structuring the zero-padded data to align with the requirements of specialized hardware units, the overhead associated with padding can be eliminated. For example, NVIDIA has introduced Sparse Tensor Core (SpTC) in its recent GPUs. When processing matrix multiplication with 2:4 structured sparsity, these sparse ALUs can skip zero elements during computation, thereby accelerating overall performance.

This paper presents SPTCStencil, a stencil computation system that transforms stencil computations into sparse matrix multiplication (SpMM) and accelerates them using sparse ALUs, eliminating the redundant workload caused by these zero values. We first propose an improved transformation scheme that converts stencil computations into general matrix multiplication. Secondly, we reorganize sparse data into 2:4 structured sparsity and encoding it to the data structure compatible with SpTC, effectively eliminate the redundant overhead incurred by padded zeros. Finally, guided by stencil workload characteristics, we optimize the computation using tiling, zero-cost row swapping, and data packing techniques, which improve execution speed while maintaining mathematical correctness.

To summarize, the contribution of this paper is as follows:

- We identify a previously overlooked structured sparsity inherent in applying stencil computation to Tensor Cores, motivating the integration of SpTCs into stencil computations for further acceleration. To our knowledge, this is the first work to exploit SpTCs for operations beyond matrix multiplication.
- We propose a novel transformation scheme that converts stencil computation into SpTC-compatible operations, successfully eliminating the redundant computation and memory access introduced by zero padding.
- We design and implement a high-performance stencil kernel featuring hierarchical tiling, zero-cost row

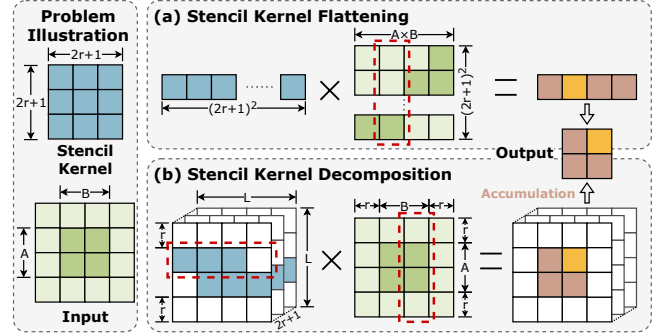


Figure 1. Optimization Paradigms for High Performance Stencil Computation.

swapping, and data packing optimizations to maximize computational efficiency.

- Experimental results show SPTCStencil outperforms SOTA CUDA Core-based solutions by 5.46× and Tensor Core-based approaches by 2.00×.

2 Background and Motivation

2.1 Stencil Computation

Stencil computation constitutes a fundamental method in scientific and engineering applications. It iteratively updates a given input domain using a predefined pattern, capturing the relevant physical phenomena or computational behaviors. It can be characterized by three aspects: the stencil shape type, dimensionality d , and radius r , also referred to as order. Stencil shapes are broadly categorized into two types: star stencils, which depend on the points along each axis; and box stencils, which depend on all the points inside the square or cubic centered around the central point. The dimensionality parameter d denotes the spatial domain of stencil operation (1D, 2D, or 3D), while the radius r , determines the spatial dependency range. For instance, a **Box-2D2R** stencil features a dependent points square of spatial dimensionality $d = 2$ and radius parameter $r = 2$, encompassing 25 points in total. For a given pattern, a stencil computation updates each input point by calculating a weighted sum over its neighboring points. The corresponding weights form a matrix known as the *stencil kernel*, which precisely defines the contribution of each neighboring point to the central point's update.

2.2 Stencil Optimizations on Tensor Cores

Traditional stencil computations rely on pointwise operations and typically leverages CUDA Cores when executed on GPUs. Recent advancements in accelerators have introduced specialized Tensor Cores, which have demonstrated approximately 4× higher performance than CUDA Cores[1]. This architectural evolution has presents new opportunities for performance optimization. To fully exploit the capabilities

of modern hardware, stencil computation paradigms must be restructured beyond their conventional formulations.

Recent research has proposed two primary optimization strategies to adapt stencil computations for efficient execution on matrix-oriented hardware, as shown in Figure 1.

Stencil Kernel Flattening. The first optimization strategy is inspired by the conceptual similarity between stencil and convolution operations. It flattens the stencil kernel into a 1D vector and reorganizes the input data accordingly using *im2col* transformation[9, 52], converting the original problem into matrix operations.

A basic transformation adopting this strategy is shown Figure 1(a). Given a Box-2D stencil, this transformation flattens the $(2r + 1) \times (2r + 1)$ stencil kernel into a vector of length $(2r + 1)^2$, while reorganizing the $A \times B$ input data into a $(2r + 1)^2 \times (A \times B)$ matrix. This transformation enables formulating the stencil update as a matrix-vector multiplication (GEMV) operation. However, directly executing this GEMV operations on Tensor Cores can result in severe hardware underutilization since Tensor Cores are designed exclusively for GEMM (General Matrix Multiplication) workloads.

ConvStencil[11] further introduces a *stencil2row* transformation that optimizes the conventional *im2col* approach by eliminating memory redundancies caused by overlapping neighborhoods in the reorganized input matrix. To maximize hardware utilization, it proposes a corresponding *dual tessellation* technique that converts GEMV operations into GEMM computations, enabling efficient Tensor Core execution tailored for this transformed data layout.

Stencil Kernel Decomposing.

The second optimization strategy tries to enable better alignment with Tensor Core compute patterns by decomposing the stencil kernel, with each decomposed substructures contributes to a partial result. Each substructures and the corresponding input are transformed into matrix multiplication separately and the partial results are accumulated later.

For example, TCStencil[28] provides a basic implementation, as shown in Figure 1(b). It decomposes the original stencil kernel by row, and replicates each row of a stencil kernel $L - 2r$ times inside a $L \times L$ matrix, allowing it to perform $L - 2r$ simultaneous updates. Crucially, this transformation recasts the computation as GEMM operations, which can be executed efficiently on Tensor Cores.

Moreover, LoRAStencil[49] specially optimized the stencil computation by assuming stencil kernels are symmetric. It applies low-rank decomposition to decompose the original stencil kernel into the sum of $r + 1$ outer product vector pairs. Then each vector pair and its corresponding input is reconstructed into GEMM operations through its *Residual Dimension Gathering* technique.

2.3 Inefficiency in Stencil Computation

Although recent studies have successfully transformed stencil computations into GEMM operations to exploit Tensor

Cores, these approaches incur significant overheads. The transformed stencil kernel matrices they construct contain a substantial proportion of zero values, resulting in both redundant computation and data movement. For example, the kernel matrices constructed via *dual tessellation* in ConvStencil are upper (or lower) triangular matrices, with half of the matrix elements are zeros. Similarly, TCStencil and LoRAStencil introduce substantial zero-padding when replicating decomposed substructures in their transformed matrices.

This section analyzes the extent of these inefficiencies for a Box-2D stencil of radius r applied over an $A \times B$ input. We establish formulations capturing the computational costs and memory access volumes to characterize the redundancy inherent in these approaches.

2.3.1 Redundant Computation. Updating a single output point in the Box-2D stencil requires at least $(2r + 1)^2$ multiply-add (MAD) operations. This establishes the following theoretical lower bound for the computational workload:

$$\text{Lower Bound}_C = AB(2r + 1)^2$$

To adapt on Tensor Cores, ConvStencil updates $8\lceil c/8 \rceil \times (2r+2)$ consecutive elements via two GEMM operations, each of size $M = 8\lceil c/8 \rceil$, $N = 8\lceil (2r + 2)/8 \rceil$, $K = 4\lceil (2r + 1)^2/4 \rceil$. Here, M, N, K represent the GEMM problem size ($\Theta_{M \times N} = \Phi_{M \times K} \times \Psi_{K \times N}$). So, we can formulate the computational workload for ConvStencil:

$$\begin{aligned} \text{ConvStencil}_C &= 512B \lceil \frac{A}{2c(r+1)} \rceil \lceil \frac{c}{8} \rceil \lceil \frac{r+1}{4} \rceil \lceil \frac{(2r+1)^2}{4} \rceil \\ &\geq 2 \text{ Lower Bound}_C \end{aligned}$$

Meanwhile, LoRAStencil updates a $c \times c$ tile through r computational stages, each comprising two GEMM operations, one of size $M = 8\lceil c/8 \rceil$, $N = 4\lceil (2r + c)/4 \rceil$, $K = 8\lceil (2r + c)/8 \rceil$, the other of size $M = 8\lceil c/8 \rceil$, $N = 4\lceil (2r + c)/4 \rceil$, $K = 8\lceil c/8 \rceil$. Thus, the computational workload for LoRAStencil is:

$$\begin{aligned} \text{LoRAStencil}_C &= 256r \frac{AB}{c^2} \lceil \frac{c}{8} \rceil \lceil \frac{2r+c}{4} \rceil \left(\lceil \frac{2r+c}{8} \rceil + \lceil \frac{c}{8} \rceil \right) \\ &\geq 1.29 \text{ Lower Bound}_C \end{aligned}$$

Similarly, TCStencil decomposes the kernel into $(2r + 1)$ rows. Each row is then encoded into a separate matrix, forming a GEMM operation with dimensions $M = N = K = L$, which update $(L - 2r)^2$ points every $(2r + 1)$ GEMM operations. Therefore, the computational workload for TCStencil is:

$$\begin{aligned} \text{TCStencil}_C &= \frac{AB}{(L - 2r)^2} L^3 (2r + 1) \\ &\geq 4.5 \text{ Lower Bound}_C \end{aligned}$$

For a stencil problem with $r = 3$, the computational workloads of ConvStencil, LoRAStencil, and TCStencil are approximately 2.12 \times , 2.94 \times , and 5.85 \times the theoretical lower bound, respectively. (For TCStencil, we use $L = 16$ to satisfy hardware constraints.)

2.3.2 Redundant Memory Access. Regarding memory access, the total memory access volume is strongly associate with the data reuse patterns. We formulate it from the perspective of input data and parameters. When updating a $c \times c$ tile, the theoretical minimum compulsory accesses require loading $(c+r)^2$ input data and $(2r+1)^2$ stencil parameters per tile. So, the lower bound for total memory access can be formulated as:

$$\text{Lower Bound}_I = AB \frac{(c+2r)^2}{c^2}$$

$$\text{Lower Bound}_P = AB \frac{(2r+1)^2}{c^2}$$

As mentioned above, ConvStencil employs two GEMM operations to update $8\lceil c/8 \rceil \times (2r+2)$ points. The memory access for ConvStencil can be written as:

$$\begin{aligned} \text{ConvStencil}_I &= 64B \lceil \frac{(2r+1)^2}{4} \rceil \lceil \frac{A}{2c(r+1)} \rceil \lceil \frac{c}{8} \rceil \\ &\geq 1.62 \text{ Lower Bound}_I \end{aligned}$$

$$\begin{aligned} \text{ConvStencil}_P &= 64B \lceil \frac{(2r+1)^2}{4} \rceil \lceil \frac{r+1}{4} \rceil \lceil \frac{A}{2c(r+1)} \rceil \lceil \frac{c}{8} \rceil \\ &\geq 2.25 \text{ Lower Bound}_P \end{aligned}$$

For each tile, LoRAStencil loads input data of size $8\lceil r/2 \rceil \times 16\lceil r/4 \rceil$ and stencil parameters of size $8 \times 8\lceil r/2 \rceil \times 2 \times r$. The entire matrix is updated in $\frac{AB}{32\lceil r/2 \rceil \lceil r/4 \rceil}$ tile computations. Thereby, the memory access for LoRAStencil is: Stencil needs $\frac{ab}{32\lceil r/2 \rceil \lceil r/4 \rceil}$ times to update the whole matrix. Each time we need to load $8\lceil r/2 \rceil \times 16\lceil r/4 \rceil$ input data and $8 \times 8\lceil r/2 \rceil \times 2 \times r$ parameters.

$$\begin{aligned} \text{LoRAStencil}_I &= 32 \frac{AB}{c^2} \lceil \frac{2r+c}{4} \rceil \lceil \frac{2r+c}{8} \rceil \\ &\geq \text{Lower Bound}_I \end{aligned}$$

$$\begin{aligned} \text{LoRAStencil}_P &= AB \frac{4r}{\lceil r/4 \rceil} \\ &\geq \frac{16}{9} \text{ Lower Bound}_P \quad (\text{for } c \geq 2) \end{aligned}$$

It should be noted that LoRAStencil exhibits lower parameter access than the theoretical lower bound when $c = 1$. This divergence arises because LoRAStencil explicitly leverages symmetric kernels within its optimization framework, whereas our lower bound derivation is established on a more general assumption, without requiring the stencil kernel to be symmetric.

Similarly, TCStencil update $(L-2r)^2$ points per tile, while loading $L^2(2r+1)$ input data and parameters. So, for TCStencil, the memory access is as follow:

$$\text{TCStencil}_I = \frac{ABL^2(2r+1)}{(L-2r)^2} \geq 3 \text{ Lower Bound}_I$$

$$\text{TCStencil}_P = \frac{ABL^2(2r+1)}{(L-2r)^2} \geq 3 \text{ Lower Bound}_P$$

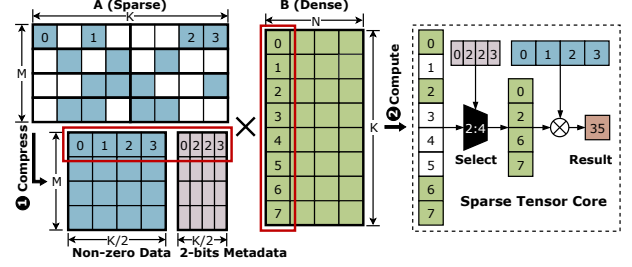


Figure 2. 2:4 Structured Sparse Format and its Compressed Representation for Sparse Tensor Core.

Having defined the memory access patterns for all methods, we can clearly demonstrate the inherent redundancy under a specific scenario. Consider a Box-2D3R stencil computation where each tile updates 8×8 points. The input memory access of ConvStencil, LoRAStencil and TCStencil 4.24 \times , 1.31 \times and 5.85 \times higher than the theoretical lower bound, and the parameter memory access is 16.98 \times , 15.67 \times and 23.41 \times higher, correspondingly. (Note: TCStencil cannot update 8×8 points due to its own design. Its measurements instead reflect a configuration updating 100 points per tile, which intrinsically improves data reuse for this method.)

This quantification reveals significant inefficiencies in both computational workloads and memory access patterns across current SOTA approaches. These fundamental limitations necessitate a new computing paradigm to minimize redundancies and unlock performance gains in stencil computations.

3 System Design

3.1 Design Rationale

Stencil computations inherently exhibit structured spatial dependencies and localized data access patterns. At each update step, only a small, spatially adjacent subset of input points contributes to the computation of a single output element. To this end, most existing GPU acceleration strategies reshape stencil kernels to fit dense computation paradigms—such as flattening into GEMV/GEMM or inflating kernel matrices via zero-padding—thereby treating the workload as if it was dense. This transformation introduces structured sparsity into the computation, but this sparsity is often overlooked, resulting in redundant memory transactions and superfluous arithmetic operations, as discussed in the previous section.

To address these inefficiencies, we reexamine stencil computation through a sparsity-centric lens. Rather than viewing zero-padding as an unavoidable overhead, we interpret it as an explicit manifestation of structured sparsity—a characteristic that can be effectively leveraged by modern hardware.

Recent GPU architectures (e.g., NVIDIA Ampere and beyond) provide native support for structured sparse matrix operations via Sparse Tensor Cores (SpTC), as illustrated in

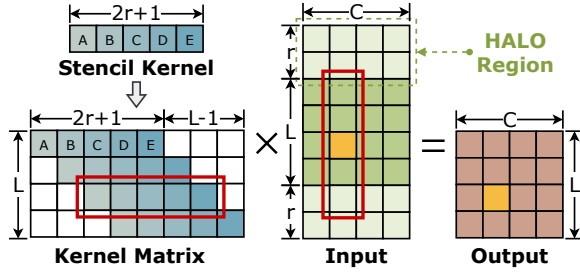


Figure 3. Matrix Multiplication with Transformed Kernel Matrix for Stencil Computation.

Figure 2. These specialized ALUs can skip zero-valued elements during matrix multiplication under a 2:4 sparsity constraint, delivering up to $2\times$ performance improvements over traditional dense tensor cores. Leveraging such hardware capabilities offers a new opportunity to accelerate stencil computations while significantly reducing both memory and computation overhead.

3.2 Strided Swapping Transformation

3.2.1 Transform to Matrix Multiplication. To fully leverage the SpTC hardware, we first transform the stencil computation into matrix multiplication operations. Our approach primarily follows the stencil kernel decomposition method described earlier in §2.2, generating partial results for each row within the stencil kernel. For conciseness, we detail the transformation methodology using a 1D stencil kernel, which corresponds to processing a single row in higher-dimensional stencil kernels. Generalizing this 1D solution to 2D or 3D stencils is then achieved by aggregating these partial results.

Given a 1D stencil kernel with radius r , we convert it into a kernel matrix with size $L \times (2r + L)$ by repeating it along the diagonal direction L times within the matrix. As illustrated in Figure 3, given the transformed kernel matrix $K \in \mathbb{R}^{L \times (2r+L)}$, a single stencil iteration computes an output matrix $Y \in \mathbb{R}^{L \times C}$ via matrix multiplication:

$$Y = K \cdot X$$

where $X \in \mathbb{R}^{(2r+L) \times C}$ is the input matrix containing the target points and their r -radius neighborhoods. For a specific output element $y_{i,j}$, its value is given by:

$$y_{i,j} = \sum_{k=1}^{2r+L} k_{i,j} \cdot x_{i,j}$$

This corresponds to the dot product between the i -th row of K and the j -th column of X . Due to the structured placement of kernel vectors, where each row i encodes the spatial offsets for the i -th output point, the operation precisely implements vertical slice stencil computation.

It should be noted that, unlike TCStencil, we do not limit the kernel matrix to be exact square. This limitation enforces

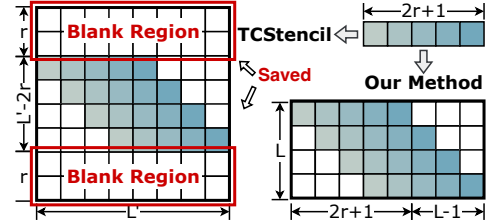


Figure 4. Matrix Multiplication with Transformed Kernel Matrix for Stencil Computation.

TCStencil to have excessive blank region on the upper and bottom side of the matrix, which is significantly inefficient. Also, we also align the kernel matrix and input matrix with the shape requirement of MMA instructions. For example, if *m8n8k4* instruction is chosen for radius 2, then the minimal size of these two matrix is then 8×12 and 12×8 .

3.2.2 Structured Sparsification. This section presents a three-step transformation scheme to adapt the kernel matrix for SpTC acceleration, as illustrated in Figure 5.

Step 1. To utilize SpTC for processing sparse data within the transformed kernel matrix, a necessary condition is that the matrix’s sparsity ratio meets the hardware requirement—specifically, exceeding 50%. The sparsity ratio of the transformed kernel matrix is defined as:

$$\text{Sparsity} = \frac{L \times (2r + 1)}{L \times (2r + L)} = \frac{2r + 1}{2r + L}$$

This formulation indicates that achieving at least 50% sparsity requires $L \geq 2r + 1$. However, sparsity ratios significantly above 50% are also undesirable, as they underutilize computational resources; SpTC can only exploit sparsity at 50%, and higher sparsity does not yield additional benefits. Therefore, we set the dimension size L to an even number $2r + 2$ to satisfy the sparsity ratio requirement while maximizing hardware utilization. The result kernel matrix is then shown in Figure 5 1.

Step 2. The transformed kernel matrix exhibits a highly regular sparsity pattern, where non-zero elements are generated through diagonal row shifting. This results in exactly $2r + 1$ non-zero elements per row, corresponding to approximately 50% sparsity per row. However, these non-zero elements are clustered rather than evenly distributed, violating hardware structural sparsity requirements. Leveraging this regularity, we transform the unstructured sparsity into structured 2:4 sparsity through column permutation. As illustrated in Figure 5, we swap odd-indexed columns j with columns $j + (2r + 2)$, while preserving even-indexed columns. This permutation ensures every contiguous 4-element segment contains at most two non-zero values, exactly satisfying the 2:4 sparse pattern required for SpTC acceleration.

A significant advantage of this permutation—which operates on the reduction dimension and requires runtime input

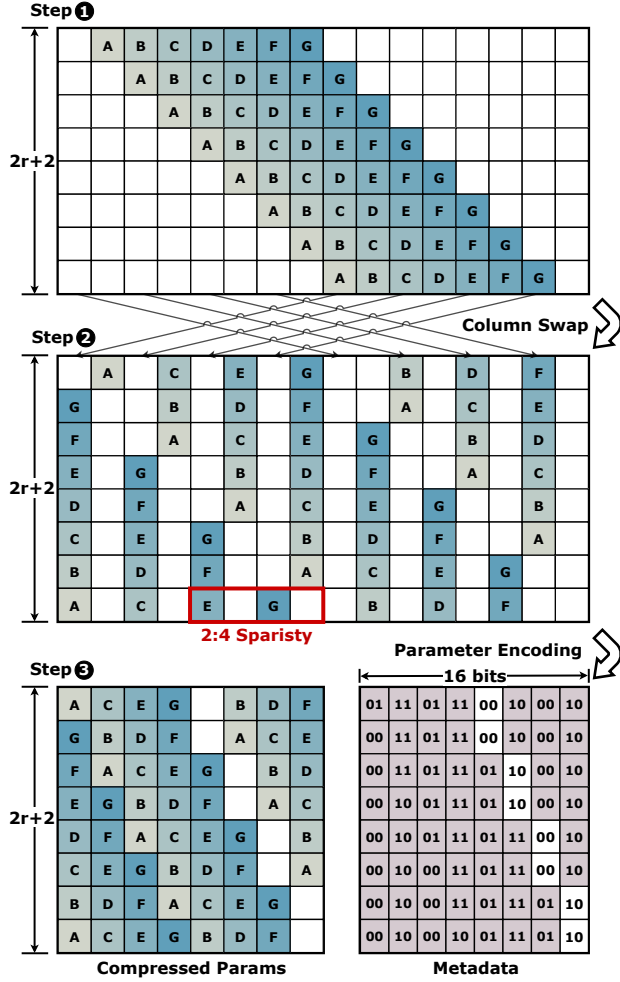


Figure 5. Sparsification and Encoding of Stencil Kernels. In this example, radius $r = 3$.

data reordering to maintain mathematical equivalence—lies in its simplicity. This characteristic enables us to integrate the necessary reordering directly into the data loading process, thereby eliminating any additional runtime overhead. Detailed implementation specifics for this runtime integration are presented in §3.3.

Step 3. The final step involves encoding the structured matrix into hardware-compatible format. As shown in Figure 5, the compression produces two outputs. First, non-zero values are compressed into the value matrix (e.g., $E0G0$ becomes EG). Second, positional metadata is generated, where the 2-bit encoding indicates the position of each non-zero within its segment. (e.g. in metadata 0010 , 00 denotes data E is at the first position in the segment.) Notably, for segment containing only one non-zero element in it, we preserve one zero placeholder in the value matrix ($00B0$), while generating metadata ($00B0$) correspondingly. This maintains consistent compression dimensions and correct

	Compute	Input Access	Param Access
Lower Bound	49	3.06	0.77
TCSStencil	286.72	17.92	17.92
ConvStencil	104	13	13
LoRAStencil	144	4	12
XXXX	56	14	7

Table 1. Quantitative Analysis of Computational and Memory Overheads for a Box-2D3R Stencil Problem.

positional encoding. All the metadata is sorted in an increasing order starting from the least significant bit within each segment.

3.2.3 Quantitative Analysis. Similar to previous formulation in §2.3, we can estimate the computational workload and memory access volume for SPTCStencil. SPTCStencil transforms the stencil computation into $2r + 1$ SpMM operations, each corresponding to a decomposed row of the stencil kernel. Specifically, for updating a tile with $c \times c$ points, the dimensions of the SpMM are $M = 8\lceil c/8 \rceil$, $N = 8\lceil c/8 \rceil$, $K = 4\lceil (2r + c)/4 \rceil$. Thereby, we can have the following expressions:

$$\begin{aligned} \text{SPTCStencil}_C &= 256 \frac{AB}{c^2} (r + 1) \left\lceil \frac{c}{8} \right\rceil^2 \left\lceil \frac{2r + c}{4} \right\rceil \\ \text{SPTCStencil}_I &= 32 \frac{AB}{c^2} (2r + 1) \left\lceil \frac{c}{8} \right\rceil \left\lceil \frac{2r + c}{4} \right\rceil \\ \text{SPTCStencil}_P &= 16 \frac{AB}{c^2} (2r + 1) \left\lceil \frac{c}{8} \right\rceil \left\lceil \frac{2r + c}{4} \right\rceil \end{aligned}$$

Having quantified the computational and memory overheads across different methods, we perform a quantitative analysis using the Box-2D3R stencil configuration. Table 1 summarizes the estimated computation and memory access costs. As demonstrated, SPTCStencil significantly outperforms all competitors in both computational workload and parameter access efficiency, leveraging our structured sparsification technique. Regarding input data access, our method either surpasses or matches alternative approaches, except for LoRAStencil. It should be emphasized that LoRAStencil is limited to symmetric stencil kernel configurations, which makes it incompatible with general stencil problems (unlike SPTCStencil), thus invalidating direct comparison.

3.3 Zero-Cost Row Swap for Mathematical Equivalent

The transformation of the kernel matrix necessitates a corresponding transformation of the input matrix to ensure computational correctness. Due to the reuse of input data across multiple computation points, data transferred to shared memory maintains the original ordering. However, this storage format requires data permutation during the shared-to-register transfer to ensure data alignment for subsequent computation. To address this challenge while preserving efficiency,

we propose a zero-cost row swap strategy that guarantees correctness without introducing additional overhead.

The shared-to-register transfer of the input matrix adheres to the MMA specification for matrix B. Each thread loads data from shared memory with specific offsets to its dedicated registers. For example, the PTX instruction of `m16n8k16` for NVIDIA SpTC requires that each thread manages four `.f16` elements in two `.f16x2` registers, with each register containing two `.f16` elements from matrix B. The thread-to-row mapping for the i -th `.f16` element follows the formulation:

$$offset_{row} = 2(lane_id \bmod 4) + 4i + (i \bmod 2)$$

where $lane_id$ represents the thread index in a wrap, ranging from 0 to 31.

For matrix multiplication in SPTCStencil, column-wise reordering of the LHS operand requires identical row-wise reordering of the RHS operand to maintain numerical equivalent. Specifically, swapping columns i and $i + L$ (where $i = 0, 2, \dots, L - 1$) in the kernel matrix mandates corresponding row swaps at positions i and $i + L$ in the input matrix. When configuring the stencil with radius $r = 7$, the structured sparse kernel matrix is constructed with $L = 16$. The equivalent matrix multiplication is split across the K dimension into two separate operations when invoking the `m16n8k16` instruction. During shared-to-register transfer, our row swap mechanism computes updated row offsets of input matrix: for the first SpTC invocation, the row offset increases by L for rows 0, 2, 4, 6; for the second SpTC invocation, the row offset decreases by L for the same rows. The updated thread-to-row mapping for the k -th SpTC invocation follows the formulation:

$$offset_{row} = 2(lane_id \bmod 4) + 4i + (i \bmod 2) + \begin{cases} 16(-1)^k, & \text{if } i \bmod 2 \equiv 0 \\ 0, & \text{if } i \bmod 2 \equiv 1 \end{cases}$$

Notably, this approach seamlessly integrates the row swap operation into the row offset computation process, thereby eliminating any additional runtime overhead while guaranteeing numerical equivalence.

3.4 High Performance Stencil Kernel Design

3.4.1 Kernel Tiling Strategy. The hierarchical GPU memory architecture, with its limited capacity at lower levels, imposes constraints on loading large data matrices. To address this challenge, tiling has become a widely adopted optimization technique that decomposes data into manageable blocks while exploiting data locality to enhance performance. Unlike conventional GEMM, the SPTCStencil kernel comprises multiple GEMM operations, each responsible for computing the outputs associated with a subset of the input. This unique characteristic necessitates a specialized tiling strategy that

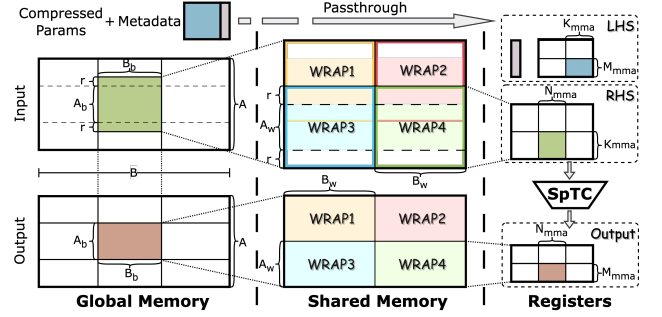


Figure 6. Tiling Strategy for Stencil Matrix Multiplication.

differs from conventional approaches, as proposed in this work and illustrated in Figure 6.

We consider a stencil operation performed on an input matrix of dimensions $A \times B$ using a 1D stencil kernel configured with radius r . The computation employs a hierarchical tiling strategy across three levels of the memory hierarchy: (1) block-level tiling for global memory access, (2) warp-level tiling for shared memory operations, and (3) mma-level tiling for thread-level register computations. Notably, due to the kernel matrix’s relatively small size compared to the input matrix and its reuse across different input blocks, the kernel matrix is only tiled at the mma level and directly loaded from global memory to registers.

For block-level tiling, the stencil kernel processes an output block of size $A_b \times B_b$, requiring the transfer of an associated input block of dimensions $(A_b + 2r) \times B_b$ that contains all input elements relevant to the computation to shared memory. This shared memory data block is further partitioned through warp-level tiling, which targets the data block being processed by 32 threads that can be simultaneously scheduled according to the SIMT execution model of NVIDIA GPUs. With tiling size $A_w \times B_w$, the input data block is iteratively loaded from shared memory to registers at the granularity of matrix multiplication. To leverage SpTC hardware for acceleration, the thread-level execution operates on mma-level tiling, aligning with the vendor-provided instruction. The instruction configuration supports matrix multiplication with dimensions $M_{mma} \times K_{mma}$ and $K_{mma} \times N_{mma}$, ensuring the data transferred to registers strictly conforms to this configuration for optimal performance.

3.4.2 Data Packing for Efficient Memory Access. Modern GPUs, as highly parallel compute accelerators, often exhibit performance bottlenecks at memory access that constrain overall throughput. To mitigate this limitation, data packing has emerged as a fundamental optimization technique in GPU kernel design. This approach reorganizes data in memory to align with GPU memory access patterns, significantly enhancing memory throughput and computational efficiency. In our SPTCStencil kernel design, matrix multiplication exhibits two key characteristics distinct from LLM

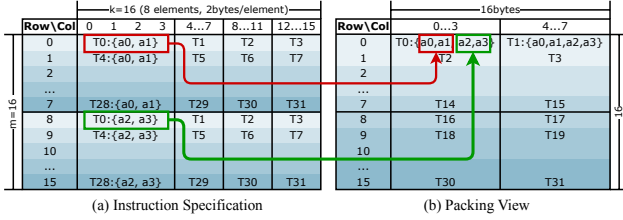


Figure 7. Data Packing for Compressed Kernel Matrix K on `mma.sp.m16n8k16` Instruction.

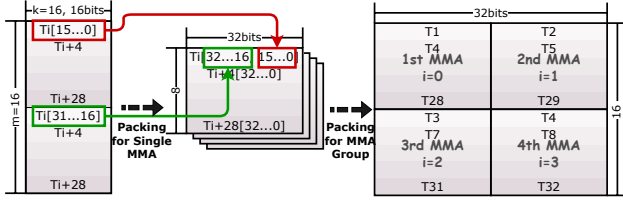


Figure 8. Metadata Matrix Data Packing and Register Reuse on `mma.sp.m16n8k16` Instruction.

applications: smaller computation scale and frequent kernel matrix reuse. Leveraging these unique characteristics and considering the underlying instruction set architecture (ISA), we propose specialized data packing strategies that aligns with GPU memory access patterns, thereby improving overall memory efficiency during kernel execution.

For global memory access, the GPU employs a coalescing mechanism that combines memory requests into memory transactions, aligning with the GPU cache line size to maximize memory efficiency. During data movement from global memory to shared memory, this coalescing mechanism is effectively utilized through block-level tiling. However, the kernel matrix, being relatively small and frequently reused, is directly loaded into registers to minimize overhead. As illustrated in Figure 7, the fragment layout for matrix A specified by SpTC introduces non-contiguous memory access patterns across threads, leading to increased memory transactions when directly loading data into registers. To address this inefficiency, we implement a specialized packing strategy that transforms the matrix into the optimized format shown in Figure 7. This packing ensures that each thread accesses contiguous memory elements, while maintaining maximum alignment with GPU memory transaction size.

Furthermore, SPTCStencil packs metadata with concatenation across multiple SpTC invocations to improve data reuse. As shown in Figure 8, the hardware accesses data from 8 threads, with the specific threads involved determined by the configuration parameter i . For instance, when i is set to 0, only threads with indices $i = 0, 4, \dots, 28$ participate in computation. However, given the GPU’s SIMD execution model, all threads load data blocks, resulting in significant data redundancy for non-computing threads. To maximize

data utilization under this configuration, we propose a metadata concatenation strategy across multiple MMA invocations. Specifically, when invoking the `mma.sp.m16n8k16` instruction, the optimal approach is to concatenate metadata matrices across four consecutive MMA invocations. This approach ensures that all loaded data contributes to computation, eliminating redundancy. The detailed packing scheme is illustrated in Figure 8. During execution, different i values are assigned to successive MMA computations to maintain proper data correspondence while fully utilizing the loaded metadata.

4 Evaluation

4.1 Evaluation Setup

Platforms. Our evaluation platform utilizes two Intel Xeon Platinum 8558P CPUs, 512GB of DDR5 memory, and four NVIDIA A100-80GB PCIe GPUs. The GPUs employ the Ampere architecture, which features dedicated SpTCs for sparse matrix computation. The system runs Ubuntu 22.04 LTS with CUDA 12.8 and cuDNN 9.8.0. Meanwhile, CPU frequency scaling is disabled across all experiments to ensure fairness.

Baselines. Our evaluation baselines encompass two categories: CUDA Core-based approaches and Tensor Core-accelerated optimizations. The former includes *cuDNN* [13], NVIDIA’s industry-standard library, which provides meticulously hand-tuned implementations of primitive operators for modern GPU architectures, and *DRStencil* [44], a SOTA framework for automatically generating and tuning highly efficient stencil code via multiple optimizations. The Tensor Core-based solutions proposed recently include *TCStencil* [28], which pioneers in conducting stencil computations on Tensor Cores; *ConvStencil* [11], which introduces a *stencil2row* transformation to minimize redundant memory accesses in general-purpose stencil operations; *LoRAStencil* [49], which leverages low-rank adaptation under symmetric kernel assumptions to further reduce memory access redundancy; and *FlashFFTStencil* [19], which employs the Fast Fourier Transform (FFT) algorithm to enhance arithmetic intensity, thereby boosting Tensor Core utilization.

It should be noted that these baseline methods are implemented using different numerical precisions: for example, *ConvStencil*, operates in FP64 precision, whereas *TCStencil* employs FP16 precision. To normalize the performance, we scale the results by a factor of 4, aligning with the approach adopted in prior work[11, 19, 49].

Benchmarks. The performance of stencil computation is evaluated through benchmarks on a series of stencil shapes, including 1D stencil kernels with radius 1 and 2, and 2D stencil kernels with two common shapes (star and box), where the radius ranges from 1 to 3.

Metrics. To quantify the performance of the stencil operation, we adopt the widely used metric in stencil computation[10,

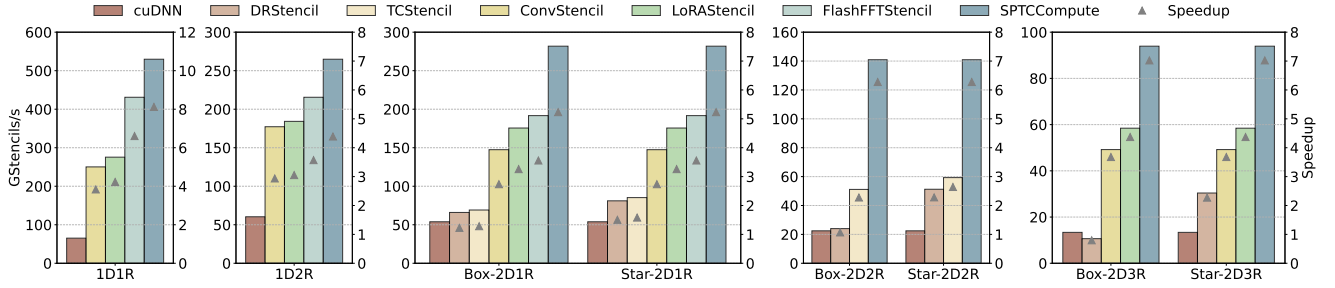


Figure 9. Performance Comparison between SPTCStencil and SOTA implementations.

31, 45–48, 50], Stencils/s (also known as Cells/s), which represents the number of stencil points updated per second. For brevity, this metric is converted to GStencils/s, where 1 GStencils/s equals 10^9 Stencils/s.

4.2 Performance Comparison

In this section, we evaluate and compare the stencil computation performance of SPTCStencil against all baseline methods across various stencil shapes. For 1D stencil shapes, we configure the problem size to 10240000 points. Meanwhile, 2D benchmarks employ a grid configuration of 10240×10240 points.

As shown in Figure 9, our approach consistently surpasses all baseline methods. Against CUDA Core-accelerated implementations, SPTCStencil delivers average speedups of $6.20\times$ over cuDNN and $4.71\times$ over DRStencil. For Tensor Core-based solutions, it achieves average speedups of $3.13\times$, $1.88\times$, $1.63\times$, and $1.35\times$ over TCStencil, ConvStencil, LoRAStencil, and FlashFFTStencil, respectively. SPTCStencil demonstrates higher throughput than existing SOTA approaches, whether optimized for memory access reduction (e.g., ConvStencil, LoRAStencil) or computational redundancy elimination (e.g., FlashFFTStencil). This dual performance advantage demonstrates the effectiveness and efficiency of SPTCStencil to resolve the fundamental inefficiency in stencil computation identified in §2.3.

Furthermore, our results demonstrate that SPTCStencil exhibits strong generalizability across all stencil shapes. First, it maintains stable performance across both box-shaped and star-shaped stencils. Unlike baselines such as DRStencil and TCStencil, which achieve higher performance on star-shaped patterns through specialized optimizations, our approach employs a general optimization strategy targeting box shapes that can be generalized to any stencil shapes. Second, SPTCStencil scales efficiently with increasing stencil order. For instance, its speedup over DRStencil increases from $4.27\times$ (Box-2D1R) to $8.82\times$ (Box-2D3R). This advantage arises because larger radius expands the optimization search space of DRStencil, leading to suboptimal implementations of the

auto-tuned kernel under fixed time constraints. SPTCStencil avoids this challenge through a predefined optimization strategy that eliminates costly search overhead.

It should be noted that our evaluation does not reflect the offline transformation overhead present in some baselines. For instance, kernels provided by DRStencil heavily depend on its tuning process, with a configurable tuning time, which is set to 1 hour in our experiments. And this tuning process is needed once the stencil kernel shape or input size changes, resulting in significant overhead beyond kernel execution time. Moreover, some baselines need comprehensive transformations when adapting to Tensor Cores. Specifically, FlashFFTStencil relies on FFT computation with $O(L^2 \log L)$ computational complexity and LoRAStencil employs low-rank adaptation with $O(L^3)$ computational complexity, incurring substantial computational overhead. In contrast, SPTCStencil incurs minimal offline transformation overhead with $O(1)$ computational complexity, as it only reorganizes stencil kernel parameters without requiring complex preprocessing operations. This efficiency further highlights SPTCStencil’s practical advantage over competing approaches when accounting for these critical preparation costs.

4.3 Performance Trend Analysis

Beyond evaluating benchmark performance on specific problem, we conduct a comprehensive analysis on the performance trend of SPTCStencil with increasing problem size. The configurations span problem sizes ranging from $1 \times (1024 \times 256)$ to $1 \times (1024 \times 4096)$ for 1D cases and 512×512 to 10240×10240 for 2D problems. While exhibiting minor deviation compared to other baselines, the evaluated problem sizes for TCStencil strictly adhere to the identical range to ensure fair comparative analysis.

As depicted in Figure 10, SPTCStencil demonstrates progressive performance gains with increasing problem size until achieving peak efficiency. Upon reaching a stable performance plateau, it consistently outperforms all baseline methods, delivering $1.86\times$ average throughput than the best-performing baseline. This scaling behavior stems from dynamic resource utilization characteristics. At smaller scales,

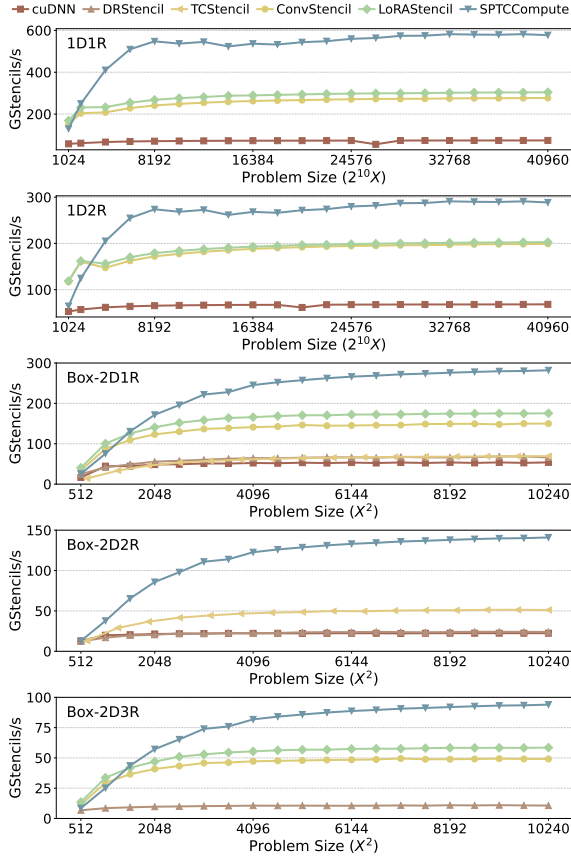


Figure 10. Performance Trend with Increasing Problem Sizes under Different Stencil Shapes.

GPU resource availability exceeds kernel demands, leading to underutilization of resources (e.g., memory bandwidth, ALUs). As problem size expands, more resources are engaged during kernel execution, enhancing GPU occupancy and thereby increasing throughput. Beyond a critical problem size, all GPU resources become saturated, limiting throughput to the peak computational capacity of the GPU—representing the theoretical performance ceiling for our approach.

Notably, SPTCStencil exhibits relatively lower performance compared to certain baselines (e.g., ConvStencil and LoRAStencil) at smaller problem sizes. This behavior originates from our optimized tiling strategy - while the larger tile configurations maximize throughput for target workloads, they initially limit parallelism extraction at reduced scales. However, this constraint is alleviated when problem sizes exceed the threshold, where hardware resources are fully utilized, shifting the bottleneck from inadequate parallelism to computational limits of GPUs. Meanwhile, beyond the performance plateau (e.g., problem size $>8192 \times 8192$ for Box-2D2R), SPTCStencil exhibits a minor yet consistent throughput gain (up to 2% measured). This results from fixed kernel

launch overheads constituting a diminishing fraction of total execution time as workloads scale.

5 Related Work

Stencil Optimizations. Traditional stencil optimizations on CPUs employ techniques such as vectorization[21, 26], tiling[7, 25, 37, 38, 41], and layout transformation[20, 21] to mitigate memory bottlenecks and enhance parallelism. For GPU architectures, researchers have developed comprehensive optimization strategies, incorporating techniques such as prefetching[36], loop unrolling[18], streaming[35, 51], and more advanced tiling techniques specifically optimized for GPUs[16, 17, 22, 30, 33, 40]. More recently, TCStencil[28] has demonstrated significant performance gains by transforming stencil computation as GEMM to leverage Tensor Cores. Building upon this approach, ConvStencil[11] and LoRAStencil[49] have optimized the transformation process for more efficient execution. Furthermore, FlashFFTStencil[19] leverages FFT to enhance arithmetic intensity and optimizes the kernel on TCs with reduced memory access.

Sparse ALU Assisted Acceleration. Sparse ALU, first introduced by NVIDIA to accelerate sparse neural networks[32], has gained widespread adoption in deep learning. The straightforward approach to leverage Sparse ALUs utilizes vendor-provided libraries like cuSPARSELt[2]. Beyond such libraries, nmSPARSE[27] implements element-wise structured sparse kernels, and DFSS [12] develops a structured sparse attention kernel. However, conventional sparse ALU requires fixed 50% sparsity. To address this, VENOM[8] and Samoyeds[43] propose flexible sparse formats supporting configurable sparsity. Concurrently, Jigsaw[50] reorders unstructured sparse data into hardware-compatible structured sparsity. Despite these advances, existing research utilizing Sparse ALUs remains primarily confined to GEMM kernels, leaving broader applicability to other computation patterns (e.g., stencil computation) unexplored.

6 Conclusion

We presented SPTCStencil, the first system leveraging Sparse Tensor Cores (SpTCs) to accelerate stencil computations, moving beyond their traditional deep learning domain. SPTCStencil efficiently transforms stencil computations into sparse matrix multiplication specifically tailored for SpTC compatibility through a novel sparsification strategy and incorporates a highly optimized GPU kernel. Experimental results show SPTCStencil outperforms SOTA CUDA Core-based solutions by 5.46 \times and Tensor Core-based approaches by 2.00 \times .

References

- [1] 2021. NVIDIA AMPERE GA102 GPU ARCHITECTURE. <https://www.nvidia.com/content/PDF/nvidia-ampere-ga-102-gpu-architecture-whitepaper-v2.pdf>.
- [2] 2024. cuSPARSELt Library. <https://docs.nvidia.com/cuda/cusparselt/>.

- [3] Kadir Akbudak, Hatem Ltaief, Vincent Etienne, Rached Abdelkhalak, Thierry Tonellot, and David Keyes. 2020. Asynchronous computations for solving the acoustic wave propagation equation. *The International Journal of High Performance Computing Applications* 34, 4 (2020), 377–393.
- [4] Yulong Ao, Chao Yang, Xinliang Wang, Wei Xue, Haohuan Fu, Fangfang Liu, Lin Gan, Ping Xu, and Wenjing Ma. 2017. 26 pflops stencil computations for atmospheric modeling on sunway taihulight. In *2017 IEEE International Parallel and Distributed Processing Symposium (IPDPS)*. IEEE, 535–544.
- [5] Krste Asanovic, Ras Bodik, Bryan Catanzaro, Joseph Gebis, Parry Husbands, Kurt Keutzer, David Patterson, William Plishker, John Shalf, and Samuel Webb Williams. 2006. The landscape of parallel computing research: A view from berkeley. (2006).
- [6] Tal Ben-Nun, Linus Groner, Florian Deconinck, Tobias Wicky, Eddie Davis, Johann Dahm, Oliver D Elbert, Rhea George, Jeremy McGibbon, Lukas Trümper, et al. 2022. Productive performance engineering for weather and climate modeling with python. In *SC22: International Conference for High Performance Computing, Networking, Storage and Analysis*. IEEE, 1–14.
- [7] Uday Bondhugula, Vinayaka Bandishti, and Irshad Pananilath. 2016. Diamond tiling: Tiling techniques to maximize parallelism for stencil computations. *IEEE Transactions on Parallel and Distributed Systems* 28, 5 (2016), 1285–1298.
- [8] Roberto L. Castro, Andrei Ivanov, Diego Andrade, Tal Ben-Nun, Basilio B. Fraguera, and Torsten Hoeftler. 2023. VENOM: A Vectorized N: M Format for Unleashing the Power of Sparse Tensor Cores. In *Proceedings of the International Conference for High Performance Computing, Networking, Storage and Analysis, SC 2023, Denver, CO, USA, November 12-17, 2023*, Dorian Arnold, Rosa M. Badia, and Kathryn M. Mohror (Eds.). ACM, 72:1–72:14. doi:10.1145/3581784.3607087
- [9] Kumar Chellapilla, Sidd Puri, and Patrice Simard. 2006. High performance convolutional neural networks for document processing. In *Tenth international workshop on frontiers in handwriting recognition*. Suvisoft.
- [10] Peng Chen, Mohamed Wahib, Shinichiro Takizawa, Ryousei Takano, and Satoshi Matsuoka. 2019. A versatile software systolic execution model for GPU memory-bound kernels. In *Proceedings of the International Conference for High Performance Computing, Networking, Storage and Analysis*. 1–81.
- [11] Yuetao Chen, Kun Li, Yuhao Wang, Donglin Bai, Lei Wang, Lingxiao Ma, Liang Yuan, Yunquan Zhang, Ting Cao, and Mao Yang. 2024. Convstencil: Transform stencil computation to matrix multiplication on tensor cores. In *Proceedings of the 29th ACM SIGPLAN Annual Symposium on Principles and Practice of Parallel Programming*. 333–347.
- [12] Zhaodong Chen, Zheng Qu, Yuying Quan, Liu Liu, Yufei Ding, and Yuan Xie. 2023. Dynamic n: M fine-grained structured sparse attention mechanism. In *Proceedings of the 28th ACM SIGPLAN Annual Symposium on Principles and Practice of Parallel Programming*. 369–379.
- [13] Sharan Chetlur, Cliff Woolley, Philippe Vandermersch, Jonathan Cohen, John Tran, Bryan Catanzaro, and Evan Shelhamer. 2014. cudnn: Efficient primitives for deep learning. *arXiv preprint arXiv:1410.0759* (2014).
- [14] Phillip Colella. 2004. Defining Software Requirements for Scientific Computing.
- [15] Chris Ding and Yun He. 2001. A ghost cell expansion method for reducing communications in solving PDE problems. In *Proceedings of the 2001 ACM/IEEE conference on Supercomputing*. 50–50.
- [16] Thomas L Falch and Anne C Elster. 2014. Register caching for stencil computations on GPUs. In *2014 16th International Symposium on Symbolic and Numeric Algorithms for Scientific Computing*. IEEE, 479–486.
- [17] Tobias Grosser, Albert Cohen, Paul HJ Kelly, Jagannathan Ramanujam, Ponuswamy Sadayappan, and Sven Verdoolaege. 2013. Split tiling for GPUs: automatic parallelization using trapezoidal tiles. In *Proceedings of the 6th Workshop on General Purpose Processor Using Graphics Processing Units*. 24–31.
- [18] Tobias Gysi, Christoph Müller, Oleksandr Zinenko, Stephan Herhut, Eddie Davis, Tobias Wicky, Oliver Fuhrer, Torsten Hoeftler, and Tobias Grosser. 2021. Domain-specific multi-level ir rewriting for gpu: The open earth compiler for gpu-accelerated climate simulation. *ACM Transactions on Architecture and Code Optimization (TACO)* 18, 4 (2021), 1–23.
- [19] Haozhi Han, Kun Li, Wei Cui, Donglin Bai, Yiwei Zhang, Liang Yuan, Yifeng Chen, Yunquan Zhang, Ting Cao, and Mao Yang. 2025. FlashFFT-Stencil: Bridging Fast Fourier Transforms to Memory-Efficient Stencil Computations on Tensor Core Units. In *Proceedings of the 30th ACM SIGPLAN Annual Symposium on Principles and Practice of Parallel Programming*. 355–368.
- [20] Tom Henretty, Kevin Stock, Louis-Noël Pouchet, Franz Franchetti, J Ramanujam, and P Sadayappan. 2011. Data layout transformation for stencil computations on short-vector simd architectures. In *Compiler Construction: 20th International Conference, CC 2011, Held as Part of the Joint European Conferences on Theory and Practice of Software, ETAPS 2011, Saarbrücken, Germany, March 26–April 3, 2011. Proceedings* 20. Springer, 225–245.
- [21] Tom Henretty, Richard Veras, Franz Franchetti, Louis-Noël Pouchet, Jagannathan Ramanujam, and Ponnuswamy Sadayappan. 2013. A stencil compiler for short-vector simd architectures. In *Proceedings of the 27th international ACM conference on International conference on supercomputing*. 13–24.
- [22] Justin Holewinski, Louis-Noël Pouchet, and Ponnuswamy Sadayappan. 2012. High-performance code generation for stencil computations on GPU architectures. In *Proceedings of the 26th ACM international conference on Supercomputing*. 311–320.
- [23] Hung T Huynh, Zhi J Wang, and Peter E Vincent. 2014. High-order methods for computational fluid dynamics: A brief review of compact differential formulations on unstructured grids. *Computers & fluids* 98 (2014), 209–220.
- [24] Mathias Jacquelin, Mauricio Araya-Polo, and Jie Meng. 2022. Scalable distributed high-order stencil computations. In *SC22: International Conference for High Performance Computing, Networking, Storage and Analysis*. IEEE, 1–13.
- [25] Guohua Jin, John Mellor-Crummey, and Robert Fowler. 2001. Increasing temporal locality with skewing and recursive blocking. In *Proceedings of the 2001 ACM/IEEE Conference on Supercomputing*. 43–43.
- [26] Kun Li, Liang Yuan, Yunquan Zhang, and Yue Yue. 2021. Reducing redundancy in data organization and arithmetic calculation for stencil computations. In *Proceedings of the International Conference for High Performance Computing, Networking, Storage and Analysis*. 1–15.
- [27] Bin Lin, Ningxin Zheng, Lei Wang, Shijie Cao, Lingxiao Ma, Quanlu Zhang, Yi Zhu, Ting Cao, Jilong Xue, Yuqing Yang, and Fan Yang. 2023. Efficient GPU Kernels for N:M-SPARSE Weights in Deep Learning. In *Sixth Conference on Machine Learning and Systems (MLSys'23)*. <https://www.microsoft.com/en-us/research/publication/efficient-gpu-kernels-for-nm-sparse-weights-in-deep-learning/>
- [28] Xiaoyan Liu, Yi Liu, Hailong Yang, Jianjin Liao, Mingzhen Li, Zhongzhi Luan, and Depei Qian. 2022. Toward accelerated stencil computation by adapting tensor core unit on GPU. In *Proceedings of the 36th ACM International Conference on Supercomputing (Virtual Event) (ICS '22)*. Association for Computing Machinery, New York, NY, USA, Article 28, 12 pages. doi:10.1145/3524059.3532392
- [29] David J Lusher, Satya P Jammy, and Neil D Sandham. 2021. OpenS-BLI: Automated code-generation for heterogeneous computing architectures applied to compressible fluid dynamics on structured grids. *Computer Physics Communications* 267 (2021), 108063.
- [30] Naoya Maruyama and Takayuki Aoki. 2014. Optimizing stencil computations for NVIDIA Kepler GPUs. In *Proceedings of the 1st international*

- workshop on high-performance stencil computations, Vienna. Citeseer, 89–95.
- [31] Kazuaki Matsumura, Hamid Reza Zohouri, Mohamed Wahib, Toshio Endo, and Satoshi Matsuoka. 2020. AN5D: automated stencil framework for high-degree temporal blocking on GPUs. In *Proceedings of the 18th ACM/IEEE International Symposium on Code Generation and Optimization*. 199–211.
- [32] Asit Mishra, Jorge Albericio Latorre, Jeff Pool, Darko Stosic, Dusan Stosic, Ganesh Venkatesh, Chong Yu, and Paulius Micikevicius. 2021. Accelerating Sparse Deep Neural Networks. arXiv:2104.08378 [cs.LG]
- [33] Anthony Nguyen, Nadathur Satish, Jatin Chhugani, Changkyu Kim, and Pradeep Dubey. 2010. 3.5-D blocking optimization for stencil computations on modern CPUs and GPUs. In *SC'10: Proceedings of the 2010 ACM/IEEE International Conference for High Performance Computing, Networking, Storage and Analysis*. IEEE, 1–13.
- [34] Long Qu, Rached Abdelkhalak, Hatem Ltaief, Issam Said, and David Keyes. 2023. Exploiting temporal data reuse and asynchrony in the reverse time migration. *The International Journal of High Performance Computing Applications* 37, 2 (2023), 132–150.
- [35] Prashant Singh Rawat, Miheer Vaidya, Aravind Sukumaran-Rajam, Mahesh Ravishankar, Vinod Grover, Atanas Rountev, Louis-Noël Pouchet, and Ponnuswamy Sadayappan. 2018. Domain-specific optimization and generation of high-performance GPU code for stencil computations. *Proc. IEEE* 106, 11 (2018), 1902–1920.
- [36] Prashant Singh Rawat, Miheer Vaidya, Aravind Sukumaran-Rajam, Atanas Rountev, Louis-Noël Pouchet, and P Sadayappan. 2019. On optimizing complex stencils on GPUs. In *2019 IEEE International Parallel and Distributed Processing Symposium (IPDPS)*. IEEE, 641–652.
- [37] Yonghong Song and Zhiyuan Li. 1999. New tiling techniques to improve cache temporal locality. *ACM SIGPLAN Notices* 34, 5 (1999), 215–228.
- [38] Robert Strzodka, Mohammed Shaheen, Dawid Pajak, and Hans-Peter Seidel. 2010. Cache oblivious parallelograms in iterative stencil computations. In *Proceedings of the 24th ACM International Conference on Supercomputing*. 49–59.
- [39] Qingxiao Sun, Yi Liu, Hailong Yang, Zhonghui Jiang, Xiaoyan Liu, Ming Dun, Zhongzhi Luan, and Depei Qian. 2021. cstuner: Scalable auto-tuning framework for complex stencil computation on gpus. In *2021 IEEE International Conference on Cluster Computing (CLUSTER)*. IEEE, 192–203.
- [40] Sven Verdoolaege, Juan Carlos Juega, Albert Cohen, Jose Ignacio Gomez, Christian Tenllado, and Francky Catthoor. 2013. Polyhedral parallel code generation for CUDA. *ACM Transactions on Architecture and Code Optimization (TACO)* 9, 4 (2013), 1–23.
- [41] Michael Wolfe. 1989. More iteration space tiling. In *Proceedings of the 1989 ACM/IEEE conference on Supercomputing*. 655–664.
- [42] David Wonnacott. 2002. Achieving scalable locality with time skewing. *International Journal of Parallel Programming* 30 (2002), 181–221.
- [43] Chenpeng Wu, Qiqi Gu, Heng Shi, Jianguo Yao, and Haibing Guan. 2025. Samoyeds: Accelerating MoE Models with Structured Sparsity Leveraging Sparse Tensor Cores. In *Proceedings of the Twentieth European Conference on Computer Systems*. 293–310.
- [44] Xin You, Hailong Yang, Zhonghui Jiang, Zhongzhi Luan, and Depei Qian. 2021. DRStencil: Exploiting data reuse within low-order stencil on GPU. In *2021 IEEE 23rd Int Conf on High Performance Computing & Communications; 7th Int Conf on Data Science & Systems; 19th Int Conf on Smart City; 7th Int Conf on Dependability in Sensor, Cloud & Big Data Systems & Application (HPCC/DSS/SmartCity/DependSys)*. IEEE, 63–70.
- [45] Liang Yuan, Shan Huang, Yunquan Zhang, and Hang Cao. 2019. Tessellating star stencils. In *Proceedings of the 48th International Conference on Parallel Processing*. 1–10.
- [46] Liang Yuan, Yunquan Zhang, Peng Guo, and Shan Huang. 2017. Tessellating stencils. In *Proceedings of the International Conference for High Performance Computing, Networking, Storage and Analysis*. 1–13.
- [47] Lingqi Zhang, Mohamed Wahib, Peng Chen, Jintao Meng, Xiao Wang, Toshio Endo, and Satoshi Matsuoka. 2023. PERKS: a locality-optimized execution model for iterative memory-bound GPU applications. In *Proceedings of the 37th International Conference on Supercomputing*. 167–179.
- [48] Lingqi Zhang, Mohamed Wahib, Peng Chen, Jintao Meng, Xiao Wang, Toshio Endo, and Satoshi Matsuoka. 2023. Revisiting temporal blocking stencil optimizations. In *Proceedings of the 37th International Conference on Supercomputing*. 251–263.
- [49] Yiwei Zhang, Kun Li, Liang Yuan, Jiawen Cheng, Yunquan Zhang, Ting Cao, and Mao Yang. 2024. LoRAStencil: Low-Rank Adaptation of Stencil Computation on Tensor Cores. In *SC24: International Conference for High Performance Computing, Networking, Storage and Analysis*. IEEE, 1–17.
- [50] Yiwei Zhang, Kun Li, Liang Yuan, Haozhi Han, Yunquan Zhang, Ting Cao, and Mao Yang. 2025. Jigsaw: Toward Conflict-free Vectorized Stencil Computation by Tessellating Swizzled Registers. In *Proceedings of the 30th ACM SIGPLAN Annual Symposium on Principles and Practice of Parallel Programming*. 481–495.
- [51] Tuowen Zhao, Protonu Basu, Samuel Williams, Mary Hall, and Hans Johansen. 2019. Exploiting reuse and vectorization in blocked stencil computations on CPUs and GPUs. In *Proceedings of the International Conference for High Performance Computing, Networking, Storage and Analysis*. 1–44.
- [52] Yangjie Zhou, Mengtian Yang, Cong Guo, Jingwen Leng, Yun Liang, Quan Chen, Minyi Guo, and Yuhao Zhu. 2021. Characterizing and Demystifying the Implicit Convolution Algorithm on Commercial Matrix-Multiplication Accelerators. arXiv:2110.03901 [cs.DC] <https://arxiv.org/abs/2110.03901>